Borja Gonzalez-Valdes, Yuri Álvarez, Spiros Mantzavinos, Carey M. Rappaport, Fernando Las-Heras, and José Ángel Martínez-Lorenzo

Improving Security Screening

A comparison of multistatic radar configurations for human body imaging.

Active millimeter-wave radar can be used for imaging concealed objects and detecting contraband at security checkpoints. Current state-of-the-art systems are based on monostatic or quasi-monostatic configurations that can misrepresent areas of the target when the specular reflection is oriented away from the incident direction. This article presents a fully multistatic millimeter-wave imaging architecture for human-body screening. Transmitters placed off the receiving aperture panel allow for maximizing the surface of the human body that can be reconstructed. A reduced number of transmitters allows for fast imaging, which minimizes the target motion effects. Multiple three-dimensional (3-D) simulation-based examples are presented to validate the proposed system.

BACKGROUND

In homeland security applications, there is increasing demand for methods to improve personnel screening for concealed object and contraband detection at security checkpoints. In this context, active nearfield millimeter-wave imaging radar systems are able to provide high-resolution imaging, with a good tradeoff between accuracy and cost. With millimeter-wave radar, the object of interest is first illuminated by millimeter waves, and then the scattered field is measured and processed to reconstruct the surface (or volume) of the object [1], [3]. The most common millimeter-wave portal imaging systems currently being used are based on monostatic radar and Fourier inversion [3]. Monostatic imaging system limitations are mainly related to the appearance of reconstruction artifacts, as described in [5]. Therefore, bistatic [6] or multistatic systems [1], [8]–[10] are useful options for improving personnel imaging.

In [2], an advanced multistatic millimeter-wave imaging configuration is presented. Multiple multistatic panels are used to create an image of the whole body. As shown in [1], the minimum number of antenna array elements is achieved when the number of transmitters is equal to the number of receivers. However, since the transmitters and receivers of each panel are

Digital Object Identifier 10.1109/MAP.2016.2569447
Date of publication: 17 June 2016

close to one another and each panel is independent from the others, this system can be seen as a quasi-monostatic approach. Although it effectively minimizes dihedral artifacts, this kind of system can misrepresent sudden indentations and protrusions in the target when the specular reflection is oriented away from the incident direction (as shown in [9, Fig. 1]). The relative position of transmitters and receivers also determines the areas of the body that the system can image, as shown in Figures 1 and 2.

This article presents a novel multistatic millimeter-wave imaging architecture for human body screening. The goal is extending, as much as possible, the imaged region by placing

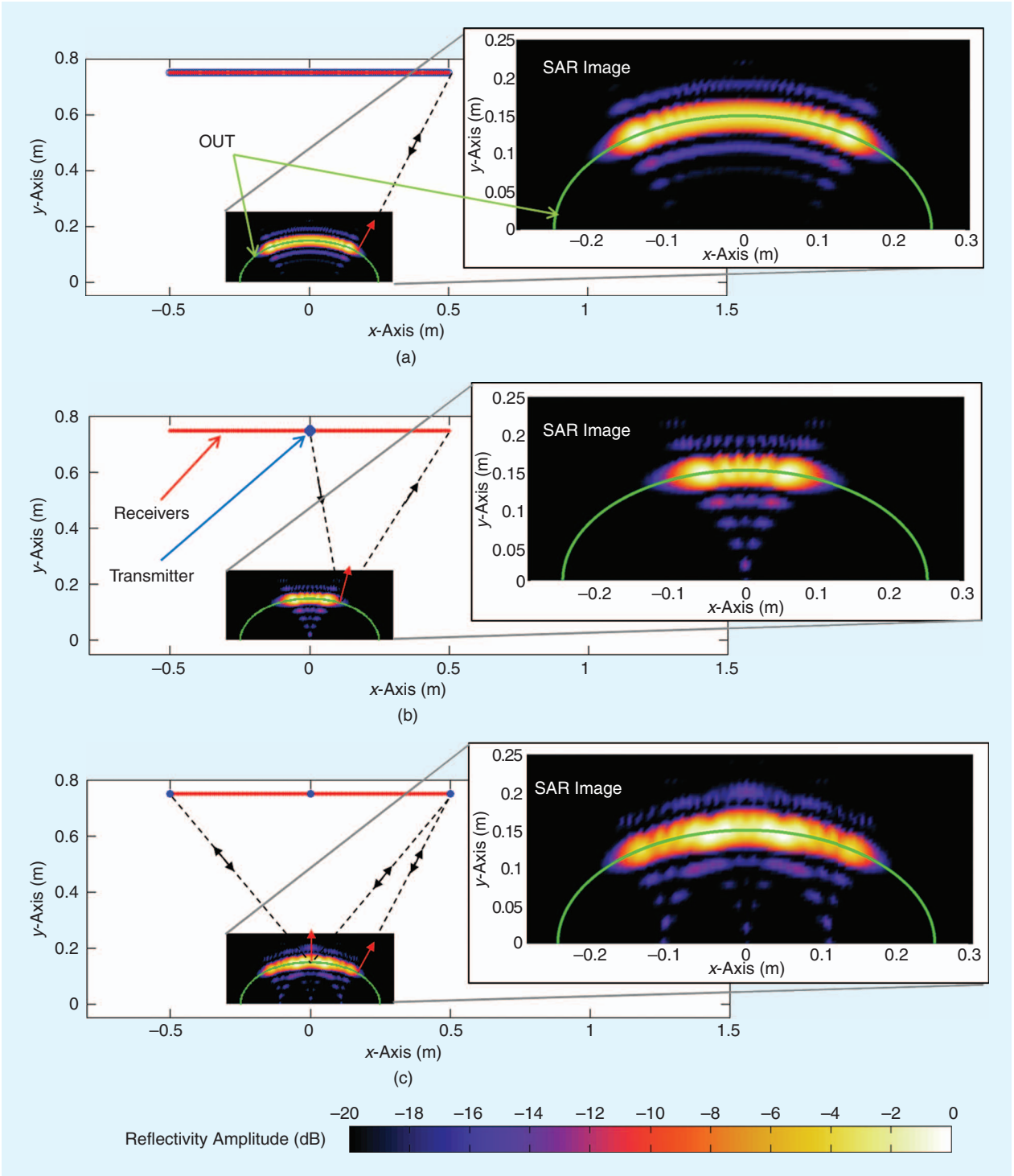

FIGURE 1. Two-dimensional (2-D) SAR imaging for different radar configurations. (a) Multimonostatic; (b) bistatic, with one transmitter in the middle of the receiving array; and (c) multistatic, with three transmitters. OUT: object-under-test, SAR: synthetic aperture radar.

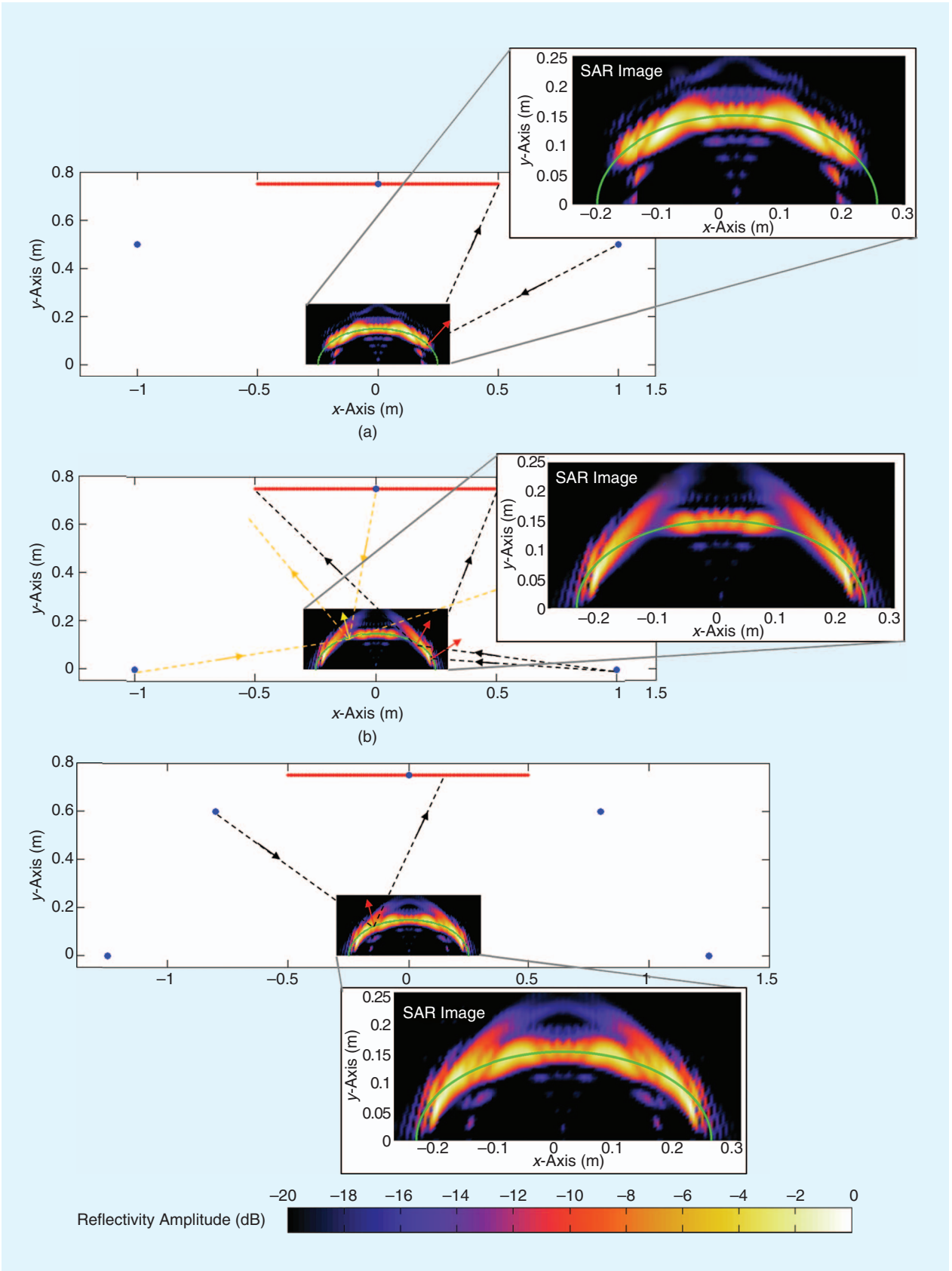

FIGURE 2. A comparison of several 2-D multistatic configurations for synthetic aperture radar (SAR) imaging. (a) Three transmitters placed at $(x,y) = (\pm 1, 0.5)$ m; (b) three transmitters placed at $(x,y) = (\pm 1, 0)$ m; and (c) five transmitters.

transmitters off the aperture panel. Fast imaging capabilities are achieved by means of Fourier-based processing as presented in [5]. Receiving arrays can be implemented by using power detectors, which are inexpensive and easy to manufacture. Concerning synthetic aperture radar (SAR) imaging, phase information can be recovered in the frequency domain, provided enough frequency bandwidth (BW) is available, as proposed in [11]. Thus, the current study is devoted to finding multistatic imaging configurations with a low number of transmitters along with the fewest possible number of receivers aiming to enlarge the imaged area with respect to current monostatic setups. Reducing the number of receiving elements is primarily accomplished by subsampling the receiving aperture. Since the transmitters need to be excited sequentially, reducing the number of transmitters also allows for faster imaging, which minimizes the target motion effects, as described in [12].

This article is focused on the comparison of several multistatic layouts for human body imaging, showing how much the imaged area can be increased. The issues of transmitter position optimization and accurate design of the receiving array are, by themselves, broad research topics that lay beyond the scope of this contribution.

IMAGING ALGORITHM

Multistatic imaging formulation needs to take into account the incident and scattered field paths, as opposed to monostatic imaging, where these paths are the same. The coordinate system is defined as: y-axis will be the range axis (depth), and x- and z-axes will be horizontal and vertical cross range. Given the reflectivity function of an object, r (x', y', z'), the field scattered on a flat receiving aperture located at $y = Y_0$ is given by

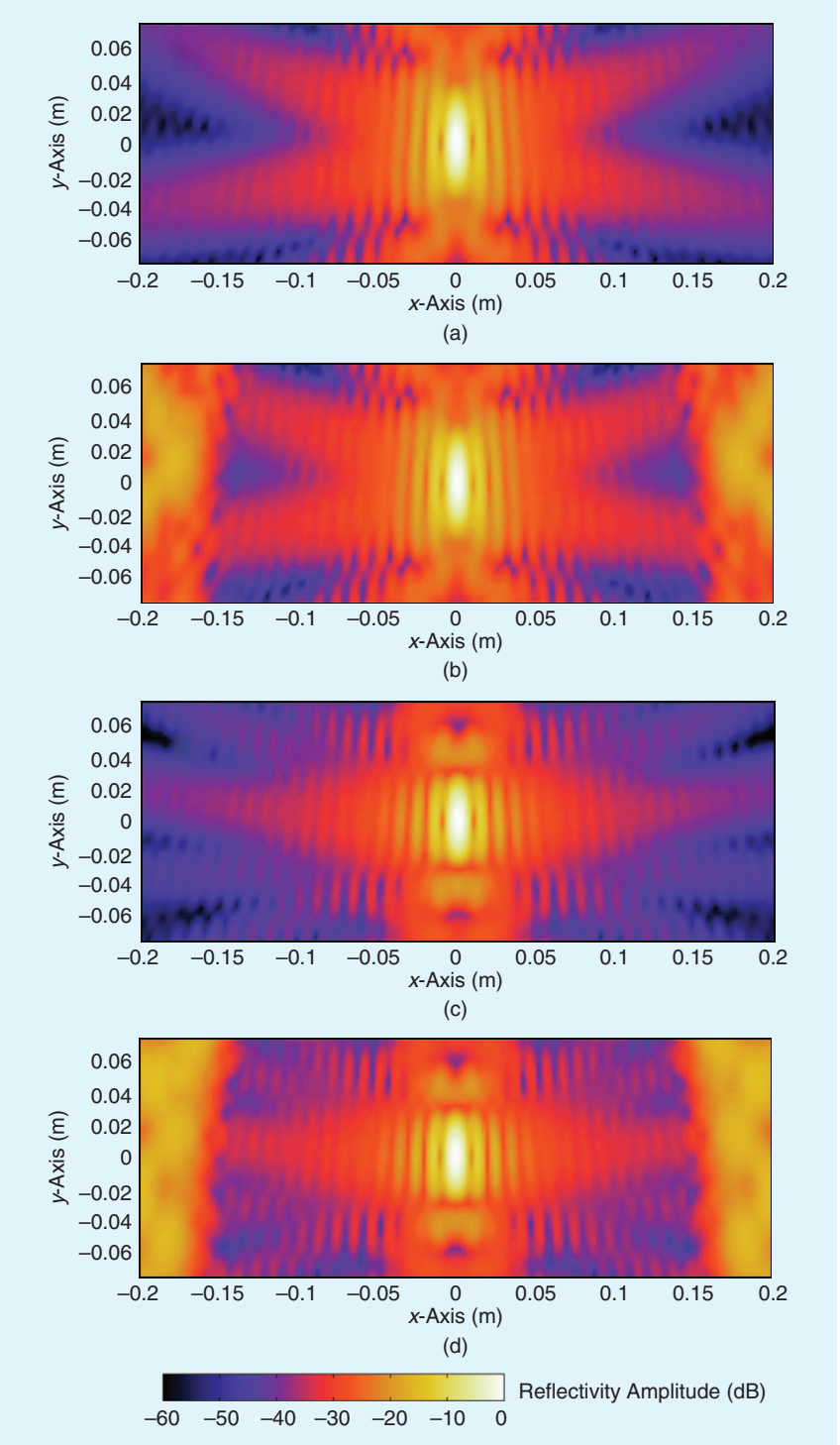

FIGURE 3. The point spread function (PSF) of the imaging configuration depicted in Figure 2(a): (a) sampling the aperture every 0.5 λ and (b) sampling the aperture every 5 λ; and the PSF of the imaging configuration depicted in Figure 1(c): (c) sampling the aperture every 0.5 λ, and (d) sampling the aperture every 5 λ.

$$E_{\text{scatt}}(f,x,z) = \int_{x'}\int_{y'}\int_{z'} \left\{ \rho(x',y',z') \cdot e^{-jk\left((x-x')^2+(Y_0-y')^2+(z-z')^2\right)^{1/2}} \cdot e^{-jk\left((x_{\text{inc}}-x')^2+(y_{\text{inc}}-y')^2+(z_{\text{inc}}-z')^2\right)^{1/2}} \right\} dz'dy'dx', \quad (1)$$

where $(x_{\text{inc}}, y_{\text{inc}}, z_{\text{inc}})$ is the position of the point source-like transmitter. Equation (1) can be effectively inverted to recover the reflectivity function from the scattered field samples collected over a given BW of frequency, yielding

the well-known SAR back-propagation imaging equation [7], [9].

$$\rho(x',y',z') = \int_x \int_z \int_f \left\{ E_{\text{scatt}}(f,x,z) \cdot e^{+jk\left((x-x')^2+(Y_0-y')^2+(z-z')^2\right)^{1/2}} \cdot e^{+jk\left((x_{\text{inc}}-x')^2+(y_{inc}-y')^2+(z_{\text{inc}}-z')^2\right)^{1/2}} \right\} dfdxdz. \quad (2)$$

Solving (2) is computationally expensive for electrically large problems. Fast integral equation-based techniques, such as the inverse fast multipole method, have been proposed [13], reducing the calculation time by several orders of magnitude. Moreover, (2) can be easily parallelized taking advantage of graphics processing unit hardware. However, these solutions are still too computationally expensive for applications requiring real-time imaging.

Monostatic setups have taken advantage of Fourier-based imaging, enabling real-time calculation [3], [4]. Even in multistatic systems as in [1], plane wave approximations can be considered to take advantage of fast calculation using FFTs. In these cases, where the large target size precludes the standard plane wave illumination assumption, a novel Fourier-based imaging technique has been proposed [5]. The idea is to decompose the imaging domain in smaller regions where the incident spherical wave can be locally treated as a plane wave. Imaging calculations for every region can be carried out in parallel, without jeopardizing the required real-time capabilities of the multistatic imaging system. Examples presented in [5] are limited to a single transmitter. The results presented in this article make use of multiple transmitters. Images produced by every transmitter are coherently combined to create the final image. Coherent combination also provides the great advantage of cancelling grating lobes due to aperture subsampling.

PROOF OF CONCEPT

MULTISTATIC SETUP

This section aims to illustrate the differences between several monostatic and multistatic radar setups [14], stating the limitations of each. The simplest case is a flat aperture receiving aperture array for sampling the scattered field. For simulation purposes, the frequency band is chosen to be 23–28 GHz; the aperture size

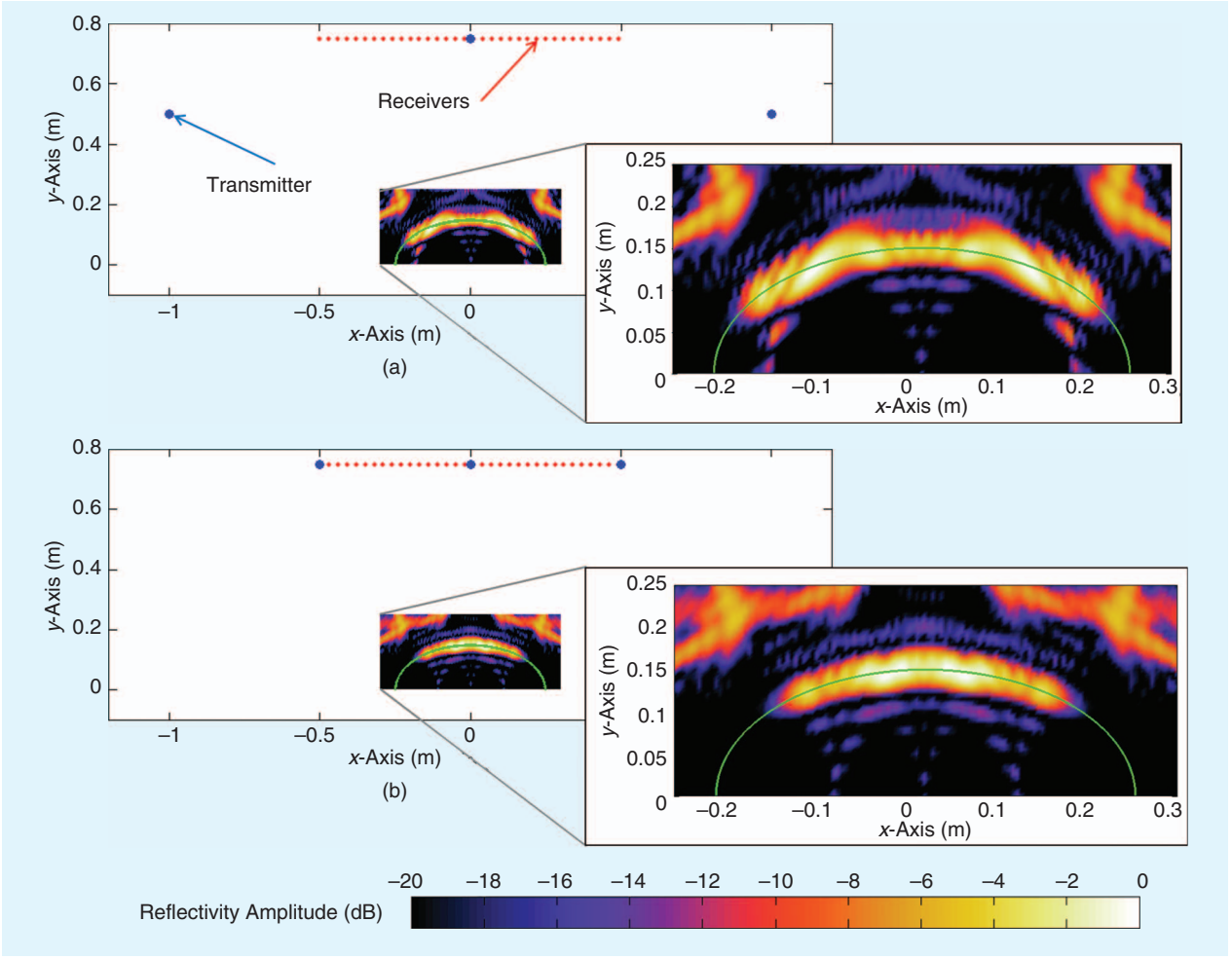

FIGURE 4. (a) SAR imaging results for the configuration depicted in Figure 2(a) when the receiving aperture is sampled every 3 λ. (b) SAR imaging results for the configuration depicted in Figure 1(c) when the receiving aperture is sampled every 3 λ.

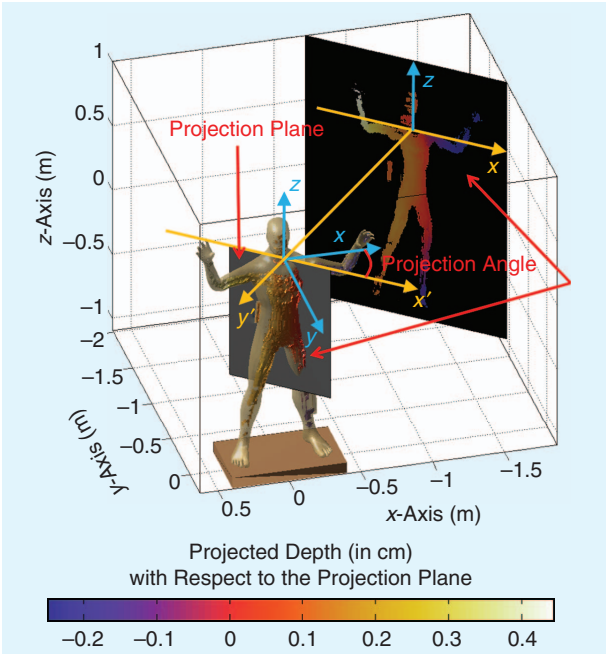

FIGURE 5. A scheme illustrating how reflectivity is projected on a projection plane, defined by a projection angle.

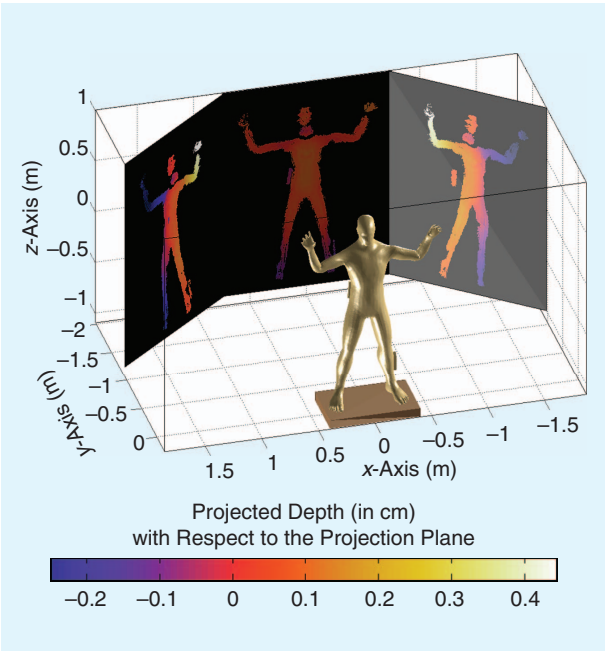

FIGURE 6. Projected reflectivity onto three different viewing planes: from left to right, projection angles are –40°, 0°, and 40°.

is 1 m, sampled every 0.5 λ at the highest frequency. The OUT is a curved metallic surface resembling the torso of the human body. The forward problem is simulated using 2-D method-of-moments. SAR images are recovered by means of standard SAR backpropagation [7], [9].

A multimonostatic radar provides twice the reconstructed imaging profile [Figure 1(a)] relative to a bistatic radar with a single transmitter placed at the middle of the receiving aperture, as depicted in Figure 1(b). In Figure 1, the true profile (shown by the green line) is reconstructed by the reflectivity map (indicated by pixel brightness). Bistatic radar imaging capabilities can be easily improved by placing two additional transmitters at the edges of the receiving aperture, as in Figure 1(c), providing the same imaging profile as the multimonostatic [Figure 1(a)]. Human body imaging has relied on monostatic [3], [4], [15] or multistatic [1], [9], [10] configurations, which are chosen based on hardware specifications rather than imaging limitations. From Figure 1, one can observe that the aperture size limits the image area of the OUT. Neither the monostatic nor the multistatic geometries are capable of providing a complete image of the OUT profile. Even if the aperture size is enlarged, it is not possible to image the entire profile, as can be easily proved with ray tracing and specular reflection.

The next step is to modify the multistatic radar by changing the placement of the transmitters while keeping the receiving aperture the same. Figure 2(a) shows the initial case: Lateral transmitters are placed off the receiving aperture. This simple change significantly enlarges the imaged region. Figure 2(b) depicts an attempt to provide full OUT imaging. However, again, ray tracing shows that specular reflection reflects away from the receiving aperture. Moreover, parts of the OUT are not imaged as the scattered field is not collected by the receiving array (plotted with dashed yellow lines).

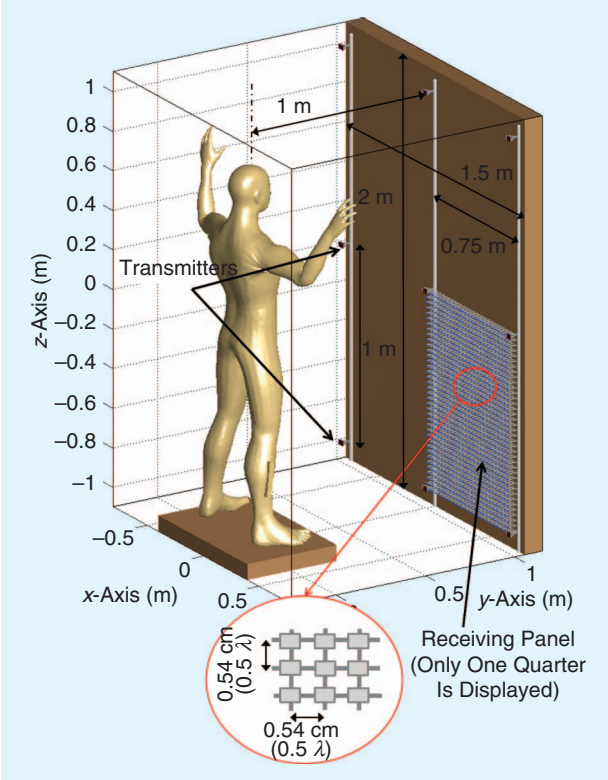

FIGURE 7. Imaging setup #1. Flat panel of receivers is placed every 0.5 λ, and nine transmitters placed in a planar layout of $(L_x, L_z) = (1.5, 2)$ m.

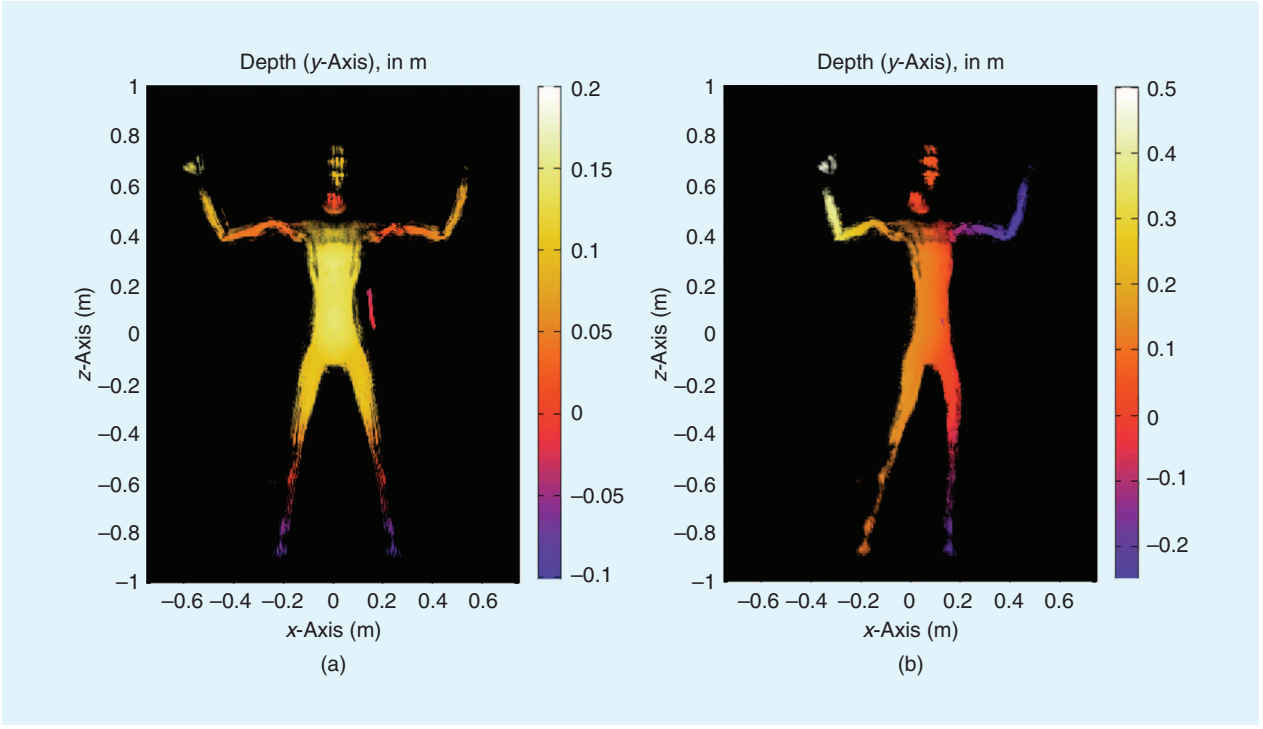

FIGURE 8. A retrieved human body image using setup #1. The color scale represents image depth in meters relative to the center of the imaging domain. (a) Projection angle 0°; (b) projection angle 40°.

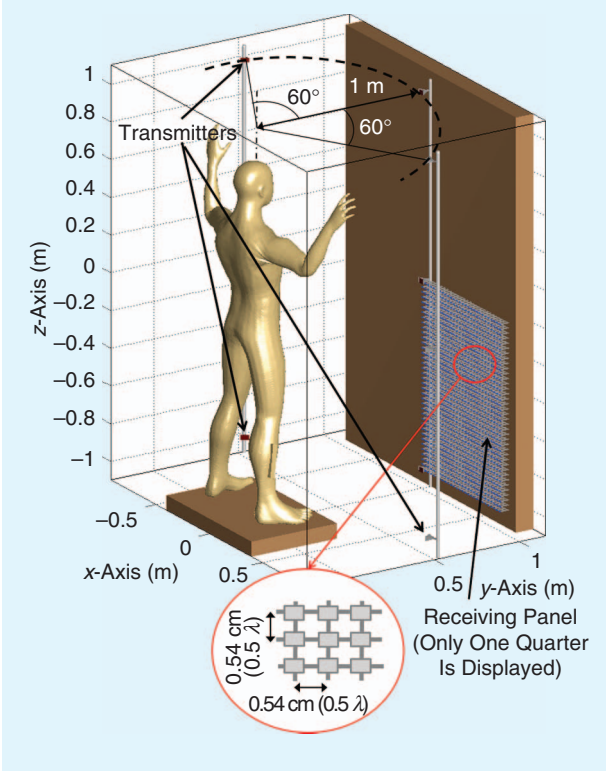

FIGURE 9. Imaging setup #2. A flat panel of receivers is placed every 0.5 λ, and nine transmitters placed in a 120°-cylindrical arc layout of R = 1 m, L_z = 2 m.

Several works [4], [9] have proposed solving this issue by means of cylindrical apertures, but again, the aperture extent limits the imaged region. As demonstrated with the results shown in Figure 2(c), this drawback can be solved by placing transmitters off the receiving aperture of the multistatic radar system, thus allowing for near complete OUT profile imaging. Concerning the quality of the recovered images, in the case of 2-D geometries, it could be assessed by applying a contour extraction method (as in [9]) then analyzing the error between the extracted contour and the true OUT profile.

RECEIVING APERTURE SUBSAMPLING

One of the main advantages of stationary imaging systems, where no movable parts are present, is the speed in acquiring scattered field samples, as well as the avoidance of mechanical maintenance. However, the tradeoff is the need for large transmitting/receiving arrays. Thus, reduction on the number of elements is a key issue for its commercial development. Several strategies, some developed in the field of antenna measurement [16], [17], have addressed this drawback. For example, use of optimal sampling interpolation methods that take into account the spatial BW of the scattered field [18] or compressed sensing techniques in the case of sparse SAR images [19]. Other approaches manipulate the imaging system point spread function (PSF) created by the transmitting and receiving arrays to cancel PSF grating lobes, successfully reducing the number of elements [1], [8], [20].

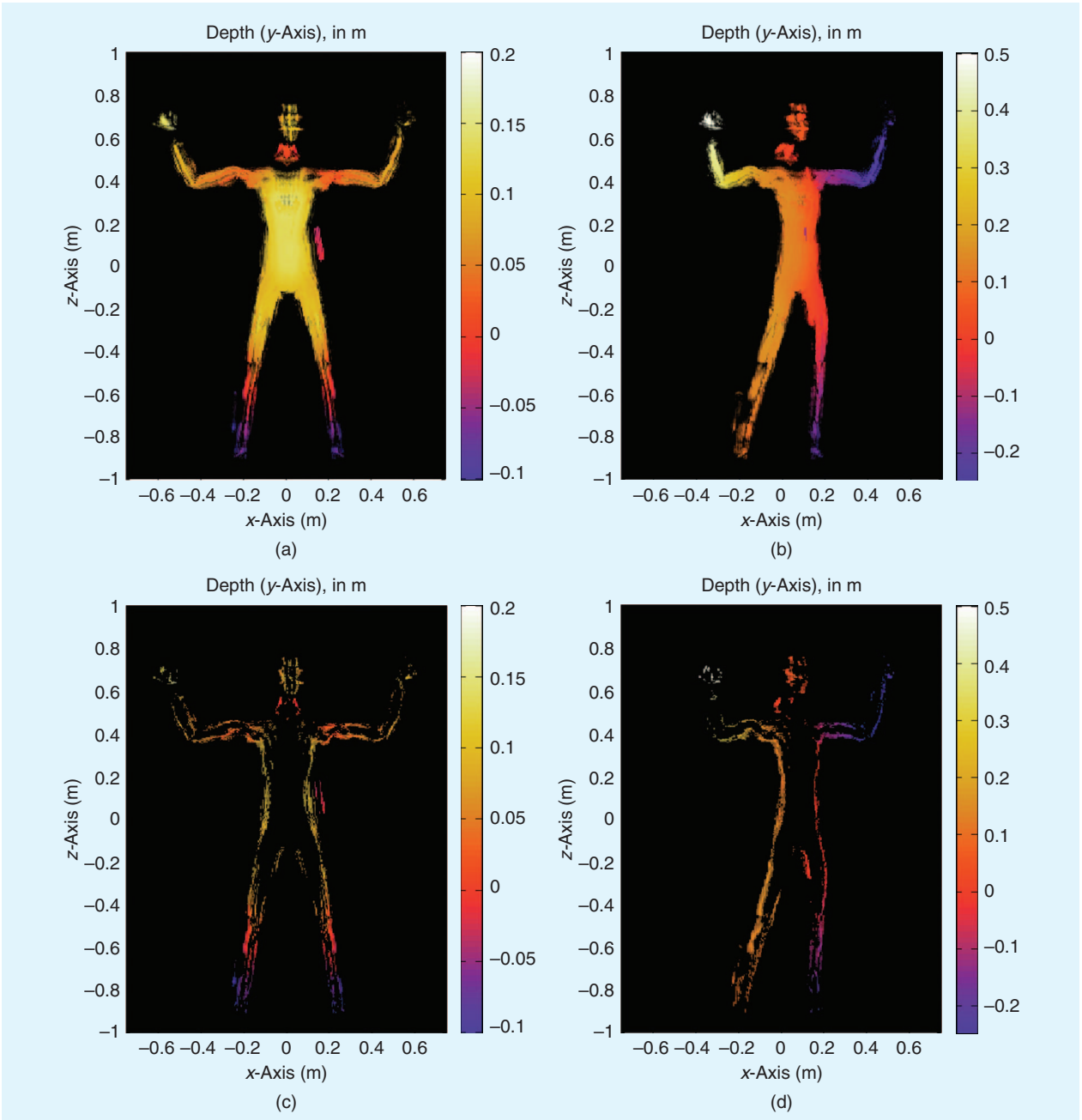

FIGURE 10. A retrieved human body image using setup #2. The color scale represents image depth in meters relative to the center of the imaging domain. (a) Projection angle 0°; (b) projection angle 40°. The improved visibility with respect to setup #1 (Figure 8) results is shown in (c) and (d).

The multistatic configurations depicted in Figure 2 cannot easily take advantage of the transmitter and receiver PSF product to cancel grating lobes, as the transmitting elements are sparsely positioned. Optimal sampling techniques would be a solution for a single transmitter, but the placement of the samples depends on the position of the illumination, so it is not valid for multiple transmitters. The solution adopted is to subsample the aperture until the PSF grating lobes appear in the imaging domain of interest. Figure 3(a) shows the PSF of the multistatic system depicted in Figure 2(a) after combining SAR images for every transmitter. When the aperture sampling rate is lowered from 0.5 λ to 5 λ, grating lobes can be observed [Figure 3(b)]. The PSF of the multistatic system plotted in Figure 1(c) is shown in Figure 3(c), where grating lobes are visible in Figure 3(d) when lowering the sampling rate from 0.5 λ to 5 λ. Practical application of subsampling is plotted in Figure 4(a) and (b) for the multistatic setups depicted in Figure 3(a) and Figure 1(c), respectively, where the aperture sampling rate is 3 λ. The profile can still be recovered, but grating lobes are visible in the imaging domain.

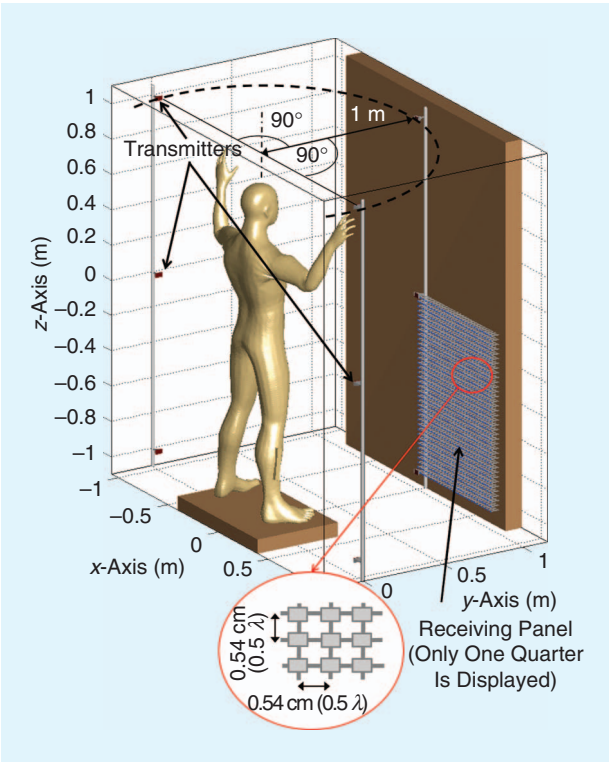

FIGURE 11. Imaging setup #3. A flat panel of receivers is placed every 0.5 m, and nine transmitters placed in a 180°-cylindrical arc layout of R = 1 m, L_z = 2 m.

In the case of the Figure 1(c) layout, grating lobes are more noticeable than in the Figure 2(a) layout.

HUMAN BODY IMAGING RESULTS

DEFINITION OF THE PROBLEM

This section quantifies the 3-D imaging performance of multistatic millimeter-wave systems according to their geometrical configuration. As stated in [3], a full-body scan requires sampling at less than one-wavelength spacing over an aperture of at least $D_x = 70$ cm wide by $D_z = 2$ m height. At $f = 25$ GHz and placing the aperture $L_y = 100$ cm away from the subject, this yields a cross-range resolution of $\delta_x = \lambda L_y / D_x = 17.1$ mm, and $\delta_z = \lambda L_y / D_z = 6$ mm, which proves to be sufficient for detecting concealed threats.

The multistatic configuration proposed in this study considers a BW of 5 GHz, from 23 to 28 GHz, yielding $\delta_y = c/\mathrm{BW} = 30$ mm range resolution. A frequency sampling rate of 250 MHz provides 60-cm range unambiguity. For this specific geometry, a flat array of receivers that is extended to 1.5 m in x-direction provides an enlarged imaging domain and higher resolution, $\delta_x = \lambda L_y / D_x = 6$ mm. In all the cases, the number of transmitters is fixed as a 3×3 elements array (that can be planar or cylindrical depending on the tested case).

The human body model considered for testing purposes (see Figure 5) has objects placed where their detection may become challenging: on the left side of the waist and on the lower part of the right leg. Due to the electrically large model to be analyzed (up to 140 λ in height for a full human body model) the forward problem is simulated using a physical optics code [21]. Noise is added to the simulated scattered field resulting in 30 dB signal-to-noise ratio (SNR).

Another issue to be addressed is related to the representation of the recovered reflectivity from the backpropagated scattered field collected on the receiving aperture. Visualization is a common problem when rendering 3-D data. It is difficult to display the relevant features of the image while maintaining the benefits of the 3-D dataset. The technique used here is called *maximum intensity projection* (*MIP*) similar to the kind of projection proposed in [1]. An MIP is a 2-D image constructed by displaying the maximum intensity along projection lines perpendicular to the viewing or projection plane, as depicted in Figure 5. The viewing plane can then be rotated around the data to provide the viewer with depth reference for image features and create a 3-D effect, as in Figure 6.

The color and opacity of each projected pixel is then mapped to the distance from a reference point and pixel intensity relative to the maximum value, respectively. In this case, the reference for depth is the center of the imaging domain. Encoding depth by color enhances the 3-D viewing effect of the rotation and provides depth data for each projected image. Encoding intensity with opacity is a natural way to let the viewer's eyes easily find the highest intensity parts of the image while also masking noisier, low amplitude areas of the image. MIP is a common imaging technique used in medical imaging and is shown to be equally effective in security imaging.

The quality of the projected image can be evaluated by means of the image SNR (ISNR), as explained in [22]. This metric is related to the sparsity of the image, as described in [19]. A similar evaluation technique is presented in [23], again focused on the evaluation of the image sparsity. However, the OUTs analyzed in [19] and [23] have a geometry simpler than the human body, where it is easier to set a correspondence between the ISNR and the quality of the image reconstruction. However, in the case of complex-geometry OUTs, as the ones presented in the "Human Body Imaging Results" section, this correspondence is not straightforward. Thus, the layouts compared in the "Human Body Imaging Results" section will be analyzed according to the human body projected area of each image.

MULTISTATIC IMAGING WITH FULL ARRAY IN RECEPTION

The first multistatic configuration (setup #1) to be tested consists of a 1.5 m width × 2 m height flat panel of receivers, placed every 10.7 mm in both directions (that is, $\lambda/2$ at 28 GHz), resulting in 104,720 elements (280×374). Nine transmitting antennas are placed as shown in Figure 7 so that the multistatic system has the same imaging area as its monostatic equivalent, as shown in the "Proof of Concept" section (Figure 1).

For every transmitter in setup #1, the amount of data to be processed is 280×374 spatial samples × 21 frequency samples ($= 222 \times 10$ scattered field samples), which also

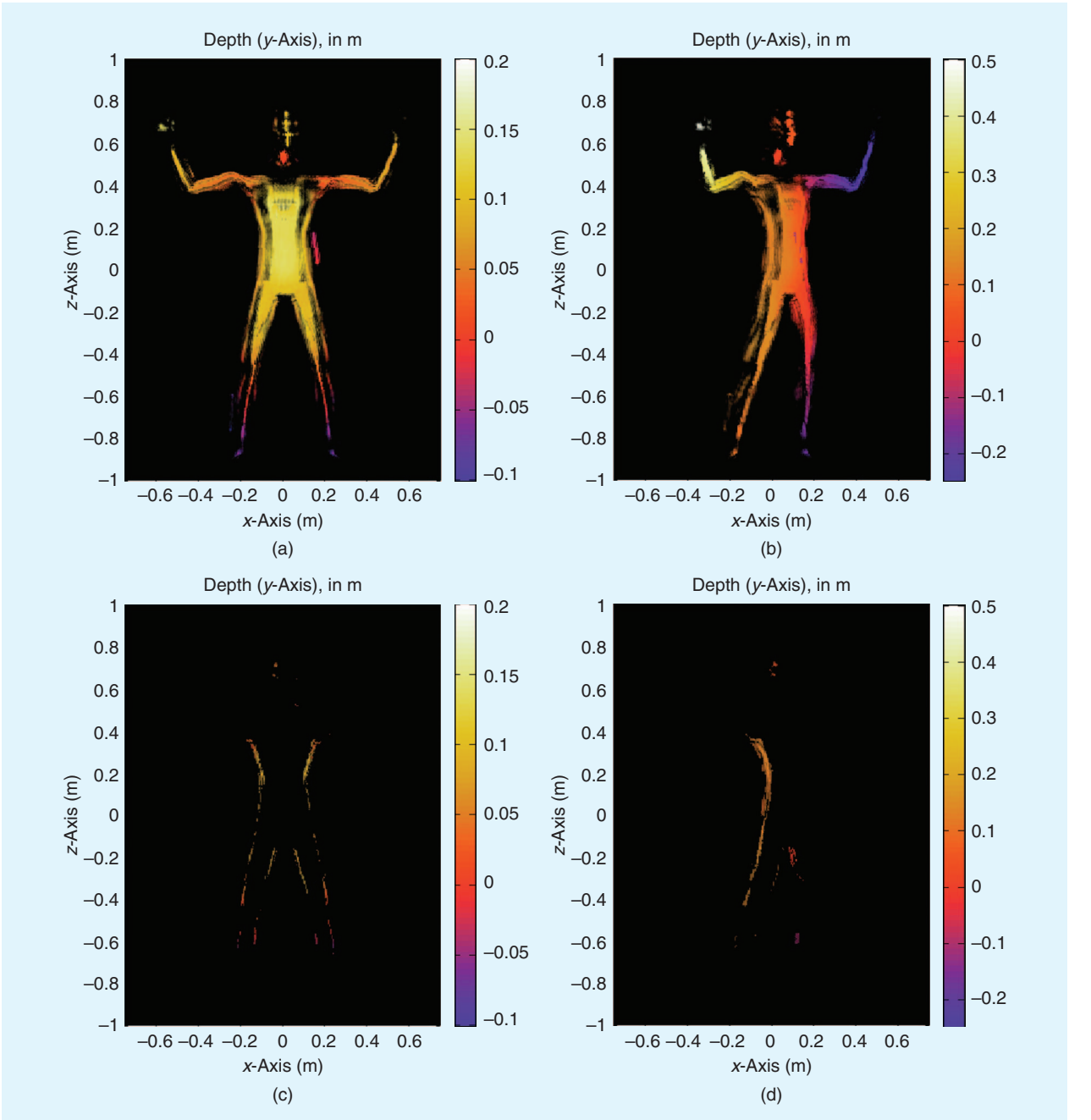

FIGURE 12. A retrieved human body image using setup #3. The color scale represents image depth, in meters relative to the center of the imaging domain. (a) Projection angle 0°; (b) projection angle 40°. The improved visibility with respect to setup #2 (Figure 10) results is shown in (c) and (d).

determines the number of imaging points in the case of Fourier-based imaging [5]. A workstation with 32 cores at 2.1 GHz and 128 GB random access memory was used for data processing. Overall calculation time for every transmitter was 45 s [5]. The processing has been run in MATLAB and has not been optimized.

Projected reflectivity for setup #1 (Figure 7) is plotted in Figure 8. Only those parts of the human body having specular reflection with any of the transmitters and receivers can be imaged. For this model, only the object on the left side of the waist is clearly visible [Figure 8(a)], whereas the object on the right leg is hardly detectable [Figure 8(b)]. These images are similar to the ones presented in [2, Fig. 4].

The next multistatic configuration analyzed (setup #2) is depicted in Figure 9. In this case, lateral transmitters are placed off the receiving aperture, as shown in Figure 2(a). With this single modification, the imaged region is enlarged, as more parts of the body will create specular reflections on the receiving aperture. This improvement is noticeable by comparing Figures 8 and 10: more parts of the body are

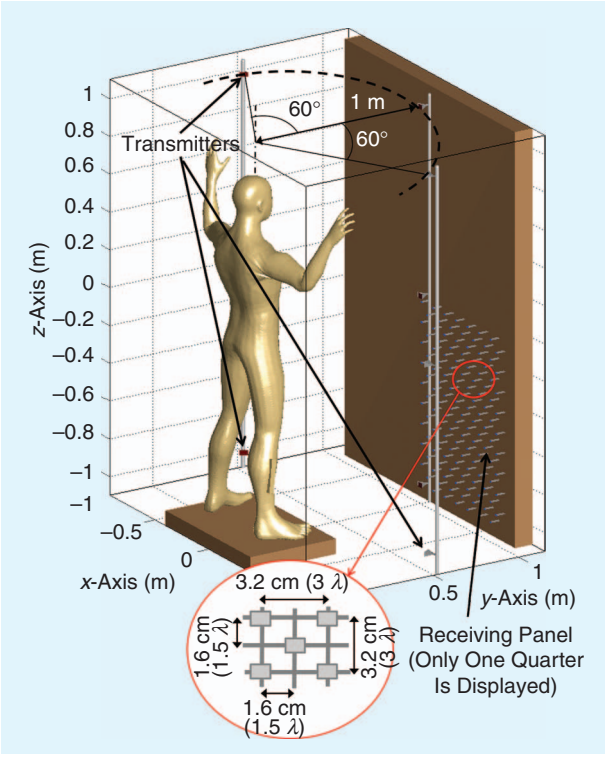

FIGURE 13. Imaging setup #4. 2 overlapping arrays of receivers, sampled every 3 λ each, and nine transmitters placed in 120°-cylindrical arc layout of R = 1 m, L_z = 2 m.

imaged in the latter, as highlighted in the differential image plotted in Figure 10(c) and (d). Of special interest is the fact that the object placed on the lower part of the right leg is clearly visible [Figure 10(b)]. A quantitative analysis of the image region enlargement based on the human body projected area is summarized in Table 1: the imaged area is increased by 37.5%.

TABLE 1. PROJECTED AREA OF THE HUMAN BODY.

Case	Projection angle 0°	Projection angle 45°
Imaging setup #1	2,454 cm	2,168 cm
Imaging setup #2	3,364 cm	2,981 cm
Imaging setup #3	3,553 cm	3,197 cm
Increment from #1 to #2	37.8%	37.5%
Increment from #2 to #3	5.6%	7.3%

Following the same argumentation as in the "Proof of Concept" section, setup #3 analyzes the case in which lateral transmitters are placed on the *x*-axis, as depicted in Figure 11. The layout of setup #3 hardly enlarges the imaged region on the sides of the human body model, as noticed in Figure 12. Quantitatively, it is about 5–7% (Table 1), significantly less than the enlargement achieved with setup #2. In addition, it creates shadow regions at about 45° and 135° in azimuth [Figure 12 (a)], visible as two dark lines on the torso that follow the vertical profile. The reason for these two shadow regions follows from the theoretical explanation given in the "Proof of Concept" section and demonstrated in Figure 2(b).

SUBSAMPLED ARRAY OF RECEIVERS

To make the imaging configuration for personnel screening feasible in terms of complexity and cost, the number of

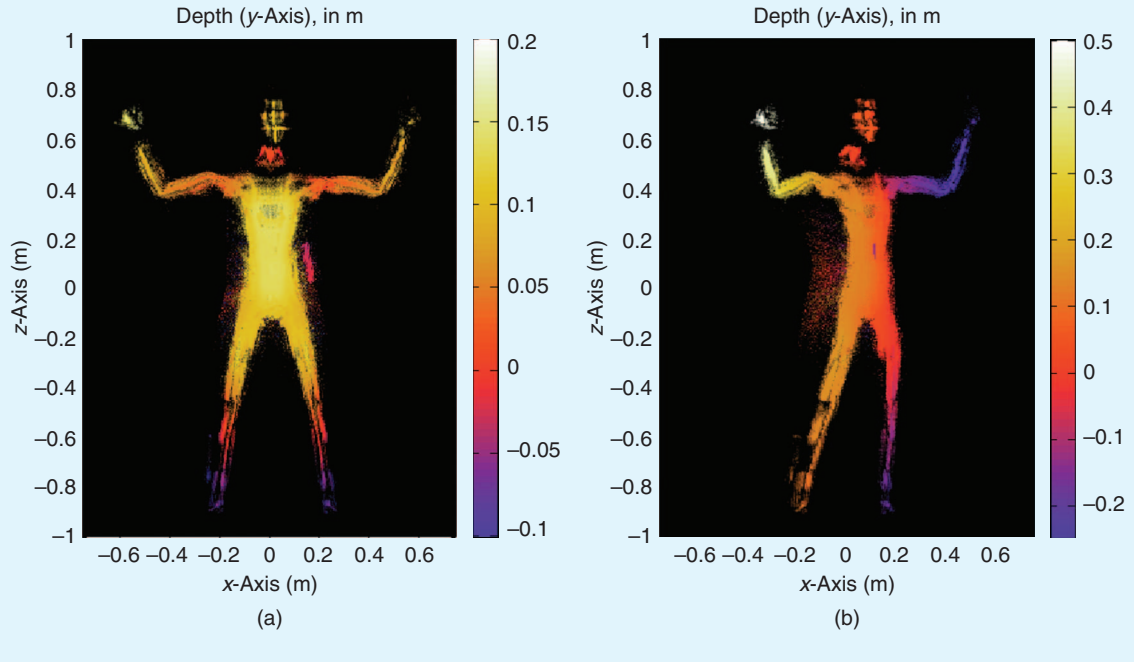

FIGURE 14. A retrieved human body image using setup #4. The color scale represents image depth, in meters, to the center of the imaging domain. (a) Projection angle 0°; (b) projection angle 40°.

TABLE 2. COMPARISON WITH SIMILAR HUMAN BODY IMAGING SYSTEMS.

Reference	$D_x \times D_z$ (cm)	$\delta_x \times \delta_z$ (mm)	Frequency band (GHz)	Number of antennas
This system, full array	150 × 200	8.0 × 6.0	23–28	104,720 Rx 9 Tx
This system, subsampled	150 × 200	8.0 × 6.0	23–28	13,090 Rx 9 Tx
MIMO array [8]	50 × 130	10.0 × 10.0	2.8–19.5	4 Tx,8 Rx, *z*-axis motion
Flat 2-D array [1]	100 × 200	3.0 × 1.5	72–80	3,072 Tx 3,072 Rx
Linear array, vertical movement [2]	72.6 Movable 2 m in z	10.0 × 3.8	27–33	66 Tx, 66 Rx, *z*-axis motion

MIMO: multiple input, multiple output; Rx: receivers; Tx: transmitters.

receivers must be kept as low as possible without compromising imaging (and thus, detection) capabilities. As discussed in the "Proof of Concept" section, due to the proposed multistatic layout, receiving aperture subsampling is the most efficient way to reduce it. A uniform grid with 13,090 receivers (setup #4) provides –28 dB grating lobe levels, which is the same order of magnitude of [1], [8]. This receiving array, shown in Figure 13, is formed from two offset overlapping arrays of receivers, each sampled every 3 λ, offset in x and z by 1.5 λ. The imaging results of setup #4 are depicted in Figure 14. Compared to Figure 10, the imaging results look noisier due to the grating lobes, but still the main features of the model are visible, certainly worth the eight times reduction in the number of receiving elements.

CONCLUSIONS

The simulation-based results presented confirm that altering the configuration of multistatic transmitter positions can significantly improve imaging by extending the reconstructed surface across more of its angular extent. That feature allows the imaging—and thus the detection—of threats that can be concealed in areas not illuminated with solely panel-based radar systems. Table 2 compares the proposed setup with already developed millimeter-wave imaging systems for security screening. Note that cross-range resolution is of the same order for each system, allowing for accurate human body imaging. The existing systems are all flat arrays and, hence, cannot image much more than ±45° [as shown in Figure 1(a)]. This is due to the specular reflection of transmitted rays missing the receiving array entirely. To accomplish 180° coverage with a flat array system, twice as many arrays would be required, whereas a full 360° reconstruction would require a square box of arrays completely enclosing the subject.

The proposed multistatic imaging architecture still requires a large number of receiving elements (13,090) if compared to other scanners with nonmovable parts such as [1]. However, from the point of view of using low-cost detectors as receivers (and even phase retrieval techniques), the proposed system has advantages due to the low number of transmitters, thus reducing technical and economical complexity. Fewer transmitters and no motion also provides faster overall scanning since only nine transmitters need to fire in sequence without repetition for the complete scan. As mentioned in the "Background" section, the next steps are devoted to optimal optimization of the transmitters' positions, as well as reducing the number of receiving array elements by means of an extended multistatic FFT algorithm capable to work with subsampled lattices.

ACKNOWLEDGMENTS

This work is supported by the Awareness and Localization of Explosives-Related Threats (ALERT) National Science Foundation's Engineering Research Centers Program (award number EEC-9986821); by the "Ministerio de Economía y Competitividad" of Spain/FEDER under project TEC2014-54005-P (MIRIIEM), project TEC2014-55290-JIN (PORTEMVISION), and project CSD2008-00068 (TERASENSE); by FEDER of the European Union and by the Principado de Asturias, through the Plan de Ciencia, Tecnología e lnnovación 2013-2017 under project GRUPIN14-114. This material is based upon work supported by the Science and Technology Directorate, U.S. Department of Homeland Security under award number "2008-ST-061-ED0001."

AUTHOR INFORMATION

Borja Gonzalez-Valdes (bgonzale@ece.neu.edu) joined the Awareness and Localization of Explosives-Related Threats Center of Excellence, Northeastern University, Boston, Massachusetts, in 2011. His research interests include antenna design, inverse scattering, radar, advanced imaging techniques, and terahertz technology. He is a Member of the IEEE.

Yuri Alvarez (yalopez@tsc.uniovi.es) is currently an assistant professor at the Signal Theory and Communications, Department of Electrical Engineering, of the University of Oviedo. He is a Senior Member of the IEEE.

Spiros Mantzavinos (smantzavinos@gmail.com) is currently an engineer with Analogic Corporation. He has been a part of the Awareness and Localization of Explosives-Related Threats team, Northeastern University, Boston, Massachusetts, developing a next-generation millimeter-wave, whole-body imaging system.

Carey M. Rappaport (rappapor@ece.neu.edu) has authored more than 400 papers in the areas of microwave antenna design, electromagnetic wave propagation and scattering computation, and bioelectromagnetics and has received several patents. He is a Fellow of the IEEE.

Fernando Las-Heras (flasheras@tsc.uniovi.es) has been a full professor at the University of Oviedo, Gijón, Spain, since December 2003. He is a Senior Member of the IEEE.

Jose A. Martinez-Lorenzo (jmartine@ece.neu.edu) has held a joint appointment in the Department of Mechanical and Industrial Engineering and Electrical and Computer Engineering as a tenure track assistant professor. He is a Member of the IEEE.

REFERENCES

[1] S. S. Ahmed, A. Schiessl, F. Gumbmann, M. Tiebout, S. Methfessel, and L. Schmidt, "Advanced microwave imaging," *IEEE Microwave Mag.*, vol. 13, no. 6, pp. 26–43, 2012.

[2] S. S. Ahmed, "Personnel screening with advanced multistatic imaging technology," *Proc. SPIE, Passive and Active Millimeter-Wave Imaging XVI*, vol. 8715, 87150B, May 2013.

[3] D. M. Sheen, D. L. McMakin, and T. E. Hall, "Three-dimensional millimeter-wave imaging for concealed weapon detection," *IEEE Trans. Microwave Theory Tech.*, vol. 49, no. 9, pp. 1581–1592, Sept. 2001.

[4] D. M. Sheen, D. L. McMakin, and T. E. Hall, "Combined illumination cylindrical millimeter-wave imaging technique for concealed weapon detection," *AeroSense, Int. Soc. Optics Photonics*, pp. 52–60, July 2000.

[5] Y. Álvarez, Y. Rodriguez-Vaqueiro, B. Gonzalez-Valdes, S. Mantzavinos, C. M. Rappaport, F. Las-Heras, and J. A. Martínez-Lorenzo, "Fourier-based imaging for multistatic radar systems," *IEEE Trans. Microwave Theory Tech.* vol. 62, no. 8, pp. 1798–1810, Aug. 2014.

[6] G. Yates, M. Horne, A. Blake, R. Middleton, and D. Andre, "Bistatic SAR image formation," *IEEE Proc. Radar Sonar Navigation*, vol. 153, no. 3, pp. 208–213, 2006.

[7] M. Soumekh, "Bistatic synthetic aperture radar inversion with application in dynamic object imaging," *IEEE Trans. Signal Processing*, vol. 39, no. 9, pp. 2044–2055, Sept. 1991.

[8] X. Zhuge and A. G. Yarovoy, "A sparse aperture MIMO-SAR-based UWB imaging system for concealed weapon detection," *IEEE Trans. Geosci. Remote Sensing*, vol. 49, no. 1, pp. 509–518, Jan. 2011.

[9] B. Gonzalez-Valdes, Y. Alvarez, J. A. Martinez, F. Las-Heras, and C. M. Rappaport, "On the use of improved imaging techniques for the development of a multistatic three-dimensional millimeter-wave portal for personnel screening," *Progress Electromagnet. Res.*, vol. 138, pp. 83–98, 2013.

[10] B. Gonzalez-Valdes, C. Rappaport, and J. A. Martinez-Lorenzo, "On-the-move active millimeter wave interrogation system using a hallway of multiple transmitters and receivers," in *Proc. 2014 IEEE Int. Symp. Antennas and Propagation*, Memphis, TN, pp. 1107–1108.

[11] J. Laviada, Y. Álvarez, C. García, C. Vázquez, S. Ver-Hoeye, M. Fernández, G. Hotopan, R. Camblor, and F. Las-Heras, "A novel phaseless frequency scanning based on indirect holography," *J. Electromagnet. Waves Appl.*, vol. 27, no. 4, pp. 275–296, 2013.

[12] A. Schiessl, S. S. Ahmed, and L.-P. Schmidt, "Motion effects in multistatic millimeter-wave imaging systems," in *Proc. SPIE, Millimetre Wave and Terahertz Sensors and Technology VI*, vol. 8900, 2013.

[13] Y. Álvarez, J. Martínez, F. Las-Heras, and C. M. Rappaport, "An inverse fast multipole method for geometry reconstruction using scattered field information," *IEEE Trans. Antennas Propagat.*, vol. 60, no. 7, pp. 3351–3360, July 2012.

[14] R. J. Burkholder, I. J. Gupta, and J. T. Johnson, "Comparison of monostatic and bistatic radar images," *IEEE Antennas Propagat. Mag.*, vol. 45, no. 3, pp. 41–50, June 2003.

[15] K. B. Cooper, R. J. Dengler, N. Llombart, B. Thomas, G. Chattopadhyay, and P. H. Siegel, "THz imaging radar for standoff personnel screening," *IEEE Trans. Terahertz Sci. Tech.*, vol. 1, no. 1, pp. 169–182, Sept. 2011.

[16] J. Laviada and F. Las-Heras, "Phaseless antenna measurement on non-redundant sample points via Leith–Upatnieks holography," *IEEE Trans. Antennas Propagat.*, vol. 61, no. 8, pp. 4036–4044, Aug. 2013.

[17] O. Bucci, C. Gennarelli, and C. Savarese, "Fast and accurate near-field far-field transformation by sampling interpolation of plane polar measurements," *IEEE Trans. Antennas Propagat.*, vol. 39, pp. 48–55, Jan. 1991.

[18] J. Laviada, Y. Álvarez, A. Arboleya, C. García-González, and F. Las-Heras, "Interferometric technique with non-redundant sampling for phaseless inverse scattering, *IEEE Trans. Antennas Propagat.*, vol. 62, no. 2, pp. 223–230, Feb. 2014.

[19] Y. Rodríguez-Vaqueiro, Y. Álvarez, B. Gonzalez-Valdes, J. A. Martínez-Lorenzo, F. Las-Heras, and C. M. Rappaport, "On the use of compressed sensing techniques for improving multistatic millimeter-wave portal-based personnel screening," *IEEE Trans. Antennas Propagat.*, vol. 62, no. 1, pp. 494–499, Jan. 2014.

[20] J. A. Martinez-Lorenzo, F. Quivira, and C. M. Rappaport, "SAR imaging of suicide bombers wearing concealed explosive threats," *Progress Electromagnet. Res.*, vol. 125, pp. 255–272, 2012.

[21] J. G. Meana, J. A. Martinez-Lorenzo, F. Las-Heras, and C. Rappaport, "Wave scattering by dielectric and lossy materials using the modified equivalent current approximation (MECA)," *IEEE Trans. Antennas Propagat.*, vol. 58, no. 11, pp. 3757–3761, Nov. 2010.

[22] W. Zhang, M. G. Amin, F. Ahmad, A. Hoorfar, and G. E. Smith, "Ultra-wideband impulse radar through-the-wall imaging with compressive sensing," *Int. J. Antennas Propagat.*, vol. 2012, no. 11, Article ID 251497, 2012.

[23] B. Gonzalez-Valdes, G. Allan, Y. Rodriguez-Vaqueiro, Y. Alvarez, S. Mantzavinos, M. Nickerson, B. Berkowitz, J. A. Martinez-Lorenzo, F. Las-Heras, and C. M. Rappaport, "Sparse array optimization using simulated annealing and compressed sensing for near-field millimeter wave imaging," *IEEE Trans. Antennas Propagat.*, vol. 62, no. 4, pp. 1716–1722, Apr. 2014.